# Application of TOPNET in the distributed model intercomparison project

Christina Bandaragoda[a,*], David G. Tarboton[a], Ross Woods[b]

[a]Utah Water Research Laboratory, Department of Civil and Environmental Engineering, Utah State University, Logan, UT 84322, USA
[b]National Institute of Water and Atmospheric Research, Christchurch, New Zealand

## Abstract

This paper describes the application of a networked version of TOPMODEL, TOPNET, as part of the Distributed Model Intercomparison Project (DMIP). The model implementation is based on a topographically derived river network with spatially distributed sub-basins draining to each network reach. The river network is mapped from the US National Elevation Dataset Digital Elevation Model (DEM) using procedures that objectively estimate drainage density from geomorphic principles. Rainfall inputs are derived from NEXRAD (radar) for each sub-basin. For each sub-basin, the wetness index distribution is derived from the DEM. The initial model parameters for each sub-basin are estimated using look up tables based on soils (STATSGO) and vegetation (1-km AVHRR). These initial model parameters provide the spatially distributed pattern of parameters at the scale of each sub-basin. Calibration uses a multiplier for each parameter to adjust the parameters while retaining the relative spatial pattern obtained from the soils and vegetation data. Parameter multipliers were calibrated using the shuffled complex evolution algorithm [J. Optim. Theory Appl. 61 (1993)] with the objective to minimize the mean square error between observed and modeled hourly streamflows. We describe the model and calibrated results submitted for all basins for the time periods involved in the DMIP study. We were encouraged by the relatively good performance of the model, especially in comparison to streamflow from smaller interior watersheds not used in calibration and simulated as ungaged basins. The limited resources used to achieve these results show some of the potential for distributed models to be useful operationally.
© 2004 Elsevier B.V. All rights reserved.

*Keywords:* Distributed; Rainfall runoff; NEXRAD; Hydrologic modeling; Ungaged basins

## 1. Introduction

We have applied a distributed version of TOPMODEL (Beven and Kirkby, 1979; Beven et al., 1995a) with a DEM-based system for delimiting channels, model components, and estimation of model parameters, to the Distributed Model Intercomparison Project (DMIP) watersheds. The implementation of TOPMODEL used is modified from the original (Beven and Kirkby, 1979; Beven et al., 1995a) by the addition of a potential evapotranspiration component, a canopy storage component to model interception, and the inclusion of a soil zone component that provides infiltration excess runoff generation capability through a Green-Ampt like parameterization.

* Corresponding author.
*E-mail address:* cmay@cc.usu.edu (C. Bandaragoda).

To parameterize the model using physical data, we used the soil texture from each of the 11 soil depth grid layers derived from Pennsylvania State University STATSGO data (Soil Survey Staff, 1994a,b) provided on the DMIP website (Smith, 2002), and soil hydraulic properties derived from texture using relationships provided by Clapp and Hornberger (1978). We also used 1 km resolution Advanced Very High Resolution Radiometer (AVHRR) vegetation data processed through the NASA Land Data Assimilation Systems (LDAS) program with an International Geosphere-Biosphere Program (IGBP) classification system (Eidenshink and Faundeen, 1994). There are a total of nine parameters that were derived from this soils and vegetation information. We used a GIS to spatially average the parameter values for each sub-basin model element.

The calibration procedure used is designed to retain the spatial pattern provided by estimating parameters from the GIS data, while still allowing an adjustment of parameters to match observed stream flow. Parameters are adjusted through a set of multipliers that scale the parameters while maintaining the relative differences between model elements indicated from the GIS information. There is one multiplier for each parameter that is the same across all sub-basins. Sub-grid variability within sub-basins is not explicitly represented apart from the spatial distribution of soil moisture that is parameterized by distribution of the TOPMODEL wetness index.

The DMIP dataset provides a unique opportunity to explore questions of location-specific radar data quality, and model performance over calibration and validation periods for different watersheds using different models. The results for our model are presented with an overview of model performance and acceptability in some watersheds, and recommendations for TOPNET model improvement in others.

We address the following questions related to the use of distributed hydrologic models. Can radar rainfall data be used for flood forecasting? Can distributed models simulate flow at uncalibrated interior locations? How applicable is a TOPMODEL representation to the DMIP watersheds? Can flows be predicted well with little or no calibration?

We found that lack of information on the uncertainty in radar rainfall inputs limits the useful interpretation of the statistical measures used to assess forecast performance. Distributed models have an advantage over lumped models in the ability to disaggregate the source of streamflow to ungaged locations upstream of the calibration location. We found that the exponential discharge–storage response function of TOPMODEL, used to model the saturated zone, limited the ability of the model to match streamflow recessions in both high flow and low flow periods. The small difference between calibrated and uncalibrated results for TOPNET showed that, in some basins, flows can be predicted well with little or no calibration. Calibration reduced the mean square errors, improving measures such as the Nash–Sutcliffe efficiency. Matching peak flows was emphasized by this approach but this was at a cost of introducing bias and poorer representation of low flows.

The following sections of this paper include a description of our model and the methods used in the DMIP experiment. Results of the DMIP experiment are given, followed by conclusions on the model performance.

## 2. Model description

TOPNET was developed by combining TOPMODEL (Beven and Kirkby, 1979; Beven et al., 1995a), which is most suited to small watersheds, with a kinematic wave channel routing algorithm (Goring, 1994) so as to have a modeling system that can be applied over large watersheds using smaller sub-basins within the large watershed as model elements. A key contribution of TOPMODEL is the parameterization of the soil moisture deficit (depth to water table) using a topographic index to model the dynamics of variable source areas contributing to saturation excess runoff. Beven et al. (1995a) indicate that "TOPMODEL is not a hydrological modeling package. It is rather a set of conceptual tools that can be used to reproduce the hydrological behavior of catchments in a distributed or semi-distributed way, in particular the dynamics of surface or sub-surface contributing areas."

The model we developed and applied here, TOPNET, uses TOPMODEL concepts for the representation of sub-surface storage controlling the dynamics of the saturated contributing area and baseflow recession. To form a complete model we
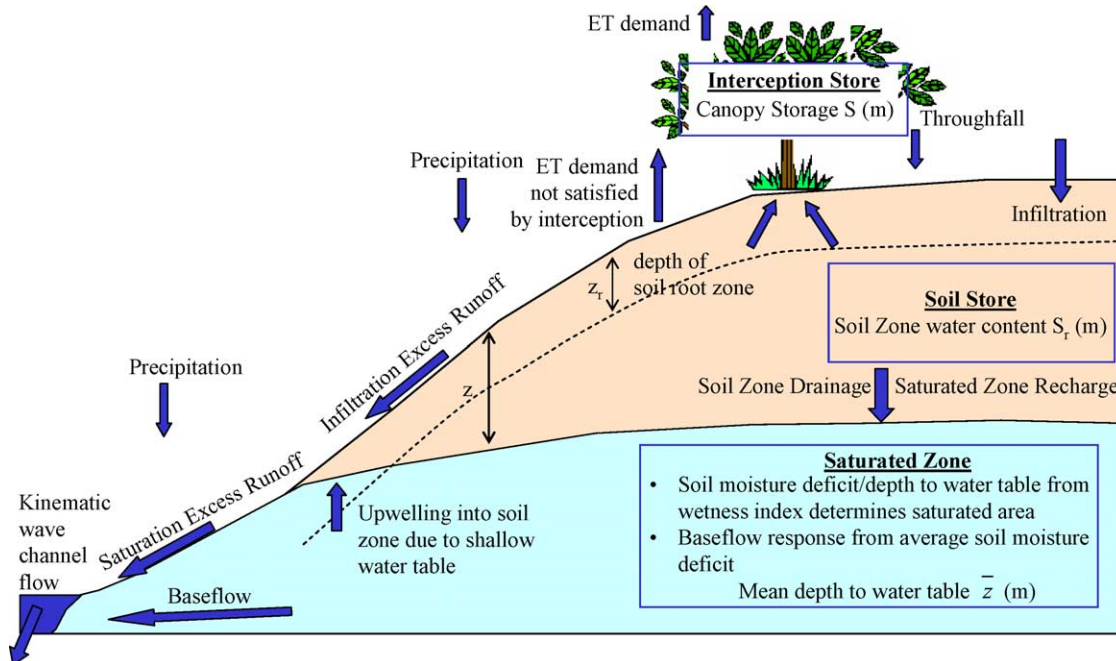
Fig. 1. Schematic of the physical processes represented by the TOPNET modeling system.

added potential evapotranspiration, interception and soil zone components. The physical processes represented in each sub-basin are shown in Fig. 1. Kinematic wave routing moves the sub-basin inputs through the stream channel network. A GIS based parameterization program, TOPSETUP, has been developed to facilitate the transformation of spatial datasets into modeling parameters and the calculation of weights associated with point precipitation measurements to provide sub-basin aggregate precipitation.

In addition to streamflow, TOPNET diagnostic output for each model element consists of time series of model state variables for each sub-basin: mean water table depth, soil zone storage, and canopy storage. Diagnostic output also includes information for each sub-basin on: infiltration excess runoff, saturation excess runoff, base flow, drainage from the soil to the saturated zone (recharge), percent saturated area, potential evapotranspiration, and actual evapotranspiration.

### 2.1. Potential evapotranspiration component

In TOPNET, potential evapotranspiration is calculated using the Priestley–Taylor equation

(Priestley and Taylor, 1972). This was chosen because it can be used with minimal input requirements of air temperature, dew point, date and time. Famiglietti et al. (1992) and Famiglietti and Wood (1994a,b) used more complete surface energy balance equations with TOPMODEL in developing the TOPLATS soil vegetation atmosphere transfer scheme (SVATS). Famiglietti's work focused on estimating evaporation fluxes as inputs to atmospheric models. We opted for a simpler approach here because the focus is on modeling runoff and because much of the data required to run a more complex SVATS model, such as wind and aerodynamic roughness is uncertain and difficult to estimate from the available data.

The available energy used in the Priestley–Taylor equation is calculated based on top of the atmosphere solar radiation forcing following procedures given in the Handbook of Hydrology (Shuttleworth, 1993) with atmospheric transmissivity estimated from the diurnal temperature range (Bristow and Campbell, 1984). Temperature and dew point for each sub-basin are estimated from nearby measurements using a lapse rate and the elevation difference between the mean sub-basin elevation and measurement elevation. In the calculation of potential evapotranspiration,

albedo and lapse rate are treated as parameters with albedo determined from land cover data.

## 2.2. Canopy interception component

The canopy interception component is a new and much simpler approach than standard interception models (e g. Rutter et al., 1972). It was developed based on the work of Ibbitt (1971) and requires only two parameters: canopy interception capacity, CC, and interception evaporation adjustment factor, $C_r$. Driving inputs to the canopy interception component are hourly precipitation and potential evapotranspiration. These are determined from the GIS land cover data. The state variable quantifying the amount of water held in interception storage, $S_i$, is used in a function $f(S_i)$ to quantify the proportion of precipitation that is throughfall (Ibbitt, 1971). The remainder $P(1 - f(S_i))$, where $P$ is precipitation rate, is added to interception storage. The same function $f(S_i)$ is used to quantify the exposure of water held in interception storage to potential evapotranspiration. Physically, $f(S_i)$ could express the fraction of leaf area that is wet, relative to its maximum. Higher rates of evaporation from interception than transpiration under the same conditions, have been suggested by Stewart (1977) and Dingman (2002). Here we represent this effect using a factor $C_r$ quantifying the increase in evaporation losses from interception relative to the potential evapotranspiration rate (Ibbitt, 1971; Stewart, 1977). The evaporation outflux from the interception store is written as $EC_rf(S_i)$ where $E$ is the potential evapotranspiration rate. The rate of change for interception storage is therefore given by

$$\frac{dS_i}{dt} = P(1 - f(S_i)) - EC_rf(S_i) \tag{1}$$

$f(S_i)$, the function giving throughfall as a function of interception storage, $S_i$, and canopy interception capacity, CC, is given by:

$$f(S_i) = \frac{S_i}{CC}\left(2 - \frac{S_i}{CC}\right) \tag{2}$$

Analytic integrals of Eq. (1) using (2) are used to solve for $S_i$ at the end of each time step to obtain the cumulative throughfall and cumulative evaporation of intercepted water. $C_r$ applies only to intercepted water, not soil water available for transpiration. Unsatisfied potential evapotranspiration demand is calculated as potential evapotranspiration minus cumulative evaporation of intercepted water divided by the interception enhancement factor $C_r$.

## 2.3. Soil component

Throughfall, $T$, and unsatisfied potential evapotranspiration, $E_p$, from the interception component serve as the forcing for the soil component, which represents the upper layer of soil to the depth below which roots can no longer extract water. Beven et al. (1995a) indicate that two formulations that have been adopted in past TOPMODEL applications have assumed that the unsaturated flows are essentially vertical and have been expressed in terms of drainage flux from the unsaturated zone. Neither of the formulations presented by Beven et al. (1995a) limit the infiltration capacity, possibly due to the historical association of TOPMODEL with the saturation excess rather than the infiltration excess runoff generation mechanism. We felt it important to accommodate both saturation and infiltration excess runoff generation mechanisms and therefore developed our own soil component that combines gravity drainage and Green-Ampt infiltration excess concepts to control the generation of surface runoff by infiltration excess as well as the drainage to the saturated zone and evapotranspiration.

Parameters describing the soil store processes are depth ($d$), saturated hydraulic conductivity ($K$), Green-Ampt wetting front suction ($\psi_f$), pore disconnectedness index soil drainage parameter ($c$), drainable porosity ($\Delta\theta_1$), and plant available porosity ($\Delta\theta_2$). The soil parameters are estimated based on soil texture from GIS soils data using relationships from Clapp and Hornberger (1978).

The state variable $S_r$ quantifies the depth of water held in the soil zone for each model element and is calculated according to

$$\frac{dS_r}{dt} = I - E_s - R \tag{3}$$

where $I$ is the infiltration rate; $E_s$, soil evaporation rate; $R$ is the drainage rate or recharge to the saturated zone store from the soil store. The infiltration rate, $I$, is limited to be less than the infiltration capacity, $I_c$,

modeled with a Green-Ampt formulation where we use the soil zone storage as infiltrated depth for the purposes of calculating $I_c$.

Unsatisfied evapotranspiration demand is given first call upon available surface water so the forcing to the soil zone is $T - E_p$. When this quantity is negative it represents evaporative demand on the soil component. When this quantity is positive it represents net surface water input that may infiltrate or become infiltration or saturation excess surface runoff.

Soil evapotranspiration is assumed to be at the potential rate when the soil moisture content is in excess of field capacity, but between field capacity and permanent wilting point, evapotranspiration is assumed to reduce linearly to zero as wilting point is approached. Soil evaporation is modeled as

$$E_s = \min\left(1, \frac{S_r}{d\Delta\theta_2}\right)(E_p - T) \tag{4}$$

for $E_p > T$ and 0 otherwise

where $E_p - T$ is the unsatisfied potential evapotranspiration demand.

We assume the soil zone is comprised of two parts, the drainable part in excess of field capacity, characterized by $\Delta\theta_1$, and the plant available moisture, characterized by $\Delta\theta_2$. Drainage is estimated as gravity drainage and is modeled to only occur when the moisture content is greater than field capacity. The relative drainable saturation, $S_{rd}$, is defined as

$$S_{rd} = \frac{\max(0, S_r - d\Delta\theta_2)}{d\Delta\theta_1} \tag{5}$$

The drainage from the soil store and recharge to the saturated zone occurs at a rate (m/h) given by

$$R = K S_{rd}^c \tag{6}$$

This is based upon a Brooks and Corey (1966) parameterization of the unsaturated hydraulic conductivity controlling the rate of drainage.

For locations with large wetness index values, the water table evaluated in the saturated zone component below may upwell into and influence the soil moisture content of the soil zone. This occurs when depth to the water table, $z$, is less than depth of the soil zone, $d$. We model the supplementary moisture in the soil zone in these cases by assuming uniform soil moisture deficit from the surface to the water table and saturated

conditions from the water table to the root zone. Thus, the shallow water table ($z < d$) increases the soil storage to

$$S_r' = S_r + (d\theta_e - S_r)\left(\frac{d - z}{d}\right) \tag{7}$$

The soil component described here was developed independently of TOPMODEL, which we used to develop the saturated zone described in Section 2.4.

### 2.4. Saturated zone component

The saturated zone component is constructed using the classical TOPMODEL assumptions of (1) saturated hydraulic conductivity decreasing exponentially with depth and (2) saturated lateral flow driven by topographic gradients at (3) steady state (Beven and Kirkby, 1979; Beven et al., 1995a). With these assumptions the local depth to the water table, $z$, is the following function of the wetness index $\ln(a/\tan\beta)$

$$z = \bar{z} + (\lambda - \ln(a/\tan\beta))/f \tag{8}$$

where $\lambda$ is the spatial average of $\ln(a/\tan\beta)$ and $\bar{z}$ the spatial average of the depth to the water table quantifying the basin average soil moisture deficit and serving as a state variable for the saturated zone component. The parameter $f$ quantifies the assumed decrease of hydraulic conductivity with depth. A histogram of wetness index values over each sub-basin is used to record the proportion of each sub-basin falling within each wetness index class. Locations, or wetness index classes, where $z$ is less than 0 as calculated using Eq. (8) are interpreted to be saturated and represent the variable source area where surface water input ($T - E_p$) becomes saturation excess runoff.

The saturated zone state equation is

$$\frac{d(\Delta\theta_1\bar{z})}{dt} = -r_{is} + T_0 e^{-\lambda} e^{-f\bar{z}} \tag{9}$$

where $r_{is}$ is the recharge, $R$, to the saturated zone averaged across wetness index classes, recognizing that for classes where the water table impacts the soil zone, $S_r$, and hence $R$, are impacted by $z$ through Eq. (7). The last term in this equation represents the per unit area baseflow, $Q_b$, draining the saturated zone

derived using the exponential decrease in hydraulic conductivity with depth assumed by TOPMODEL, with $T_0$ being transmissivity

$$Q_b = T_0 \, e^{-\lambda} \, e^{-f\bar{z}} \qquad (10)$$

In solving the model we do not save a state variable either for the saturated zone or soil zone for each wetness index class. Rather we only save state variables $\bar{z}$ and $S_r$ for each sub-basin. At each time step, Eq. (8) gives the depth to the water table for a specific wetness index class within a sub-basin, and Eq. (7) gives the modification of $S_r$ for wetness index classes impacted by a shallow water table. This approach is different from the Beven version of TOPMODEL (Beven et al., 1995b) where a separate soil zone is modeled for each wetness index class. We felt that keeping track of state variables at scales smaller than the basic sub-basin model element introduces unnecessary complexity and is unwarranted. If smaller spatial resolution is required to provide more explicit resolution of spatial variability, then smaller sub-basins can be delineated.

### 2.5. Routing component

There are three sources of runoff from each sub-basin; (1) saturation excess runoff from excess precipitation on variable source saturated areas as determined from the topographic wetness index, (2) infiltration excess runoff as determined from the Green-Ampt parameterization based upon soil zone storage and (3) base flow representing saturated zone drainage according to Eq. (10). This runoff is delayed in reaching the outlet due to the time taken by within sub-basin travel, as well as travel in the stream network to the overall watershed outlet. Within sub-basin travel is modeled assuming a constant hillslope velocity, $V$, which is a calibrated input parameter. A histogram of the down slope flow distances from each grid cell in each sub-basin to the first stream encountered is derived from the GIS and used to perform this routing.

Once in the stream, a kinematic wave routing algorithm (Goring, 1994) is used to route flow through the network. Sub-basin inputs to the channel network are assumed to occur at the head of first order streams and at the midpoint of internal stream reaches. Fig. 2

gives an example of the sub-basins used to model flow in the Illinois River at Tahlequah. The inset on Fig. 2 gives the schematic channel network with sub-basin inputs used to route flow for the portion of this network draining to the interior gage at Savoy. The parameters used in the kinematic wave channel network routing are Manning's roughness parameter $n$, as well as width, slope and length for each channel segment. Slope and length are determined from the GIS based upon the Digital Elevation Model (DEM). Channel width is determined as a power function of contributing area (Leopold and Maddock, 1953) fit to data from New Zealand rivers.

### 2.6. Precipitation interpolation

TOPNET is configured to derive aggregated sub-basin precipitation inputs as a weighted sum of point precipitation measurements. The weights associated with each gauge for each sub-basin are calculated as part of the preprocessing by TOPSETUP using linear interpolation based upon Delauney triangles. In the DMIP application, the center points of NEXRAD radar grid cells were used as precipitation gage locations. With this input, TOPSETUP determines the set of weights used to estimate sub-basin precipitation in terms of individual NEXRAD radar grid cells.

## 3. The DMIP experiment

Results were submitted to the National Weather Service (NWS) for the period June 1, 1993–July 31, 2001 with May 1, 2000–July 31, 2001 serving as a validation period. Our group submitted both calibrated and uncalibrated results for all five basins, all interior locations within each of the five basins (Reed et al., 2003), and over the entire calibration and validation period requested by the NWS. The difference between calibrated and uncalibrated simulations showed how simulations improved with calibration specific to a particular basin. With calibration using streamflow measurements at basin outlets, model predictions reported at interior locations can test the ability of distributed models to predict flow at ungaged locations. With model calculations performed at an hourly time step,
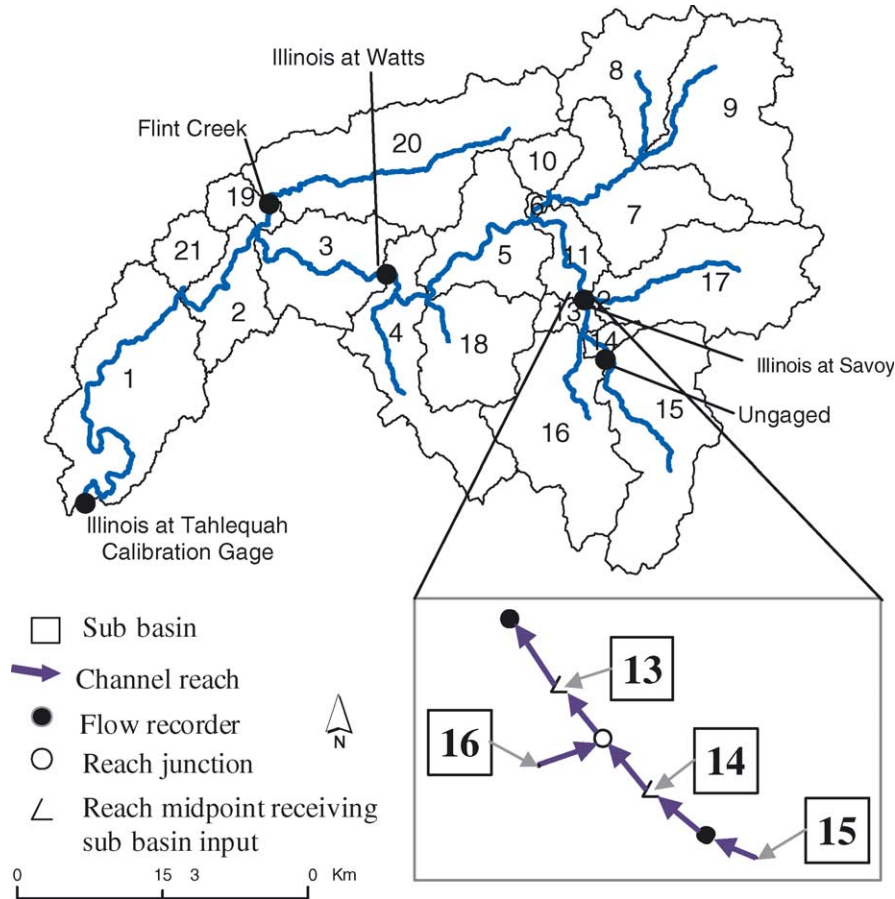
Fig. 2. Model element distribution for the watershed of the Illinois River at Tahlequah. Channel routing of flow from sub-watersheds through the channel system is displayed for the interior gage at Savoy.

results can be analyzed in terms of usefulness and acceptability for multiple uses, including flood forecasting.

### 3.1. Spatial configuration

To delineate streams and sub-basins we used the 30 m resolution National Elevation Dataset DEM (USGS, 2003) for this region. Software developed by Tarboton (2002) was used to filter the DEM, remove pits and calculate the single (D8) flow direction and contributing drainage area associated with each grid cell. The curvature based drainage network delineation method described by Tarboton and Ames (2001) was used to delineate streams. This method delineates the highest resolution stream

network statistically consistent with empirical geomorphologic laws, specifically the constant drop property (Broscoe, 1959) which is related to Horton's slope and length laws and the power law relationship between stream slope and drainage area (Flint, 1974). The average drainage density that resulted was $0.4 \, km^{-1}$ for the DMIP watersheds. The resulting channel network was visually checked against digital raster graph images of USGS 1:24,000 topographic maps.

The DMIP stream gage and ungaged simulation point locations were all found to lie on third or higher order streams. To reduce the number of model elements involved we generalized the delineated stream network by eliminating all first and second order streams. The DEM flow direction grid was
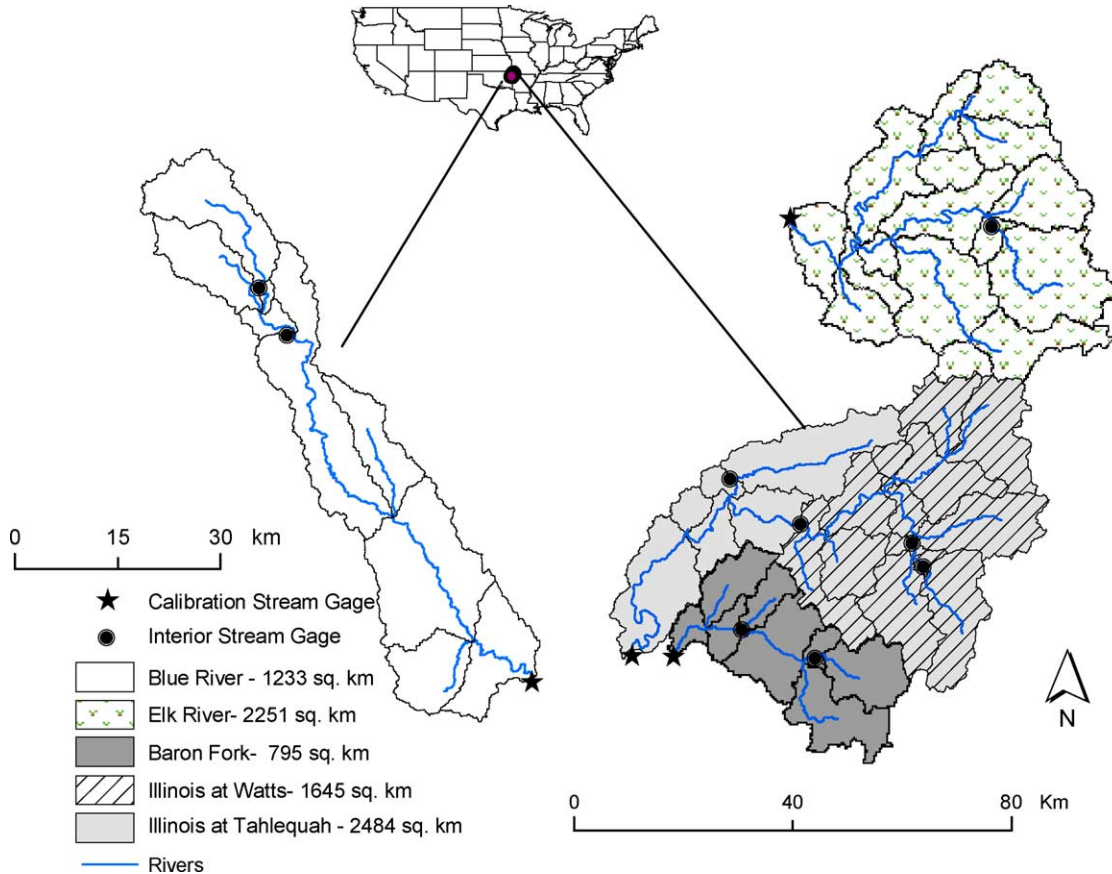
Fig. 3. DMIP river basins are located in the south central United States and range in size from 800 to 2500 km². Interior gaged locations were modeled as 'ungaged' for the experiment. The Illinois at Tahlquah basin includes the Illinois at Watts basin. The Illinois at Watts streamgage location was used once as an interior 'ungaged' location for modeling Illinois at Tahlequah, and secondly for the calibration of Illinois at Watts.

then used to delineate the sub-basin draining directly to each third or higher order stream reach. These sub-basins are shown in Fig. 3 and were used as model elements in TOPNET. The average size of the model elements was 90 km².

The $D_{\infty}$ multiple flow direction algorithm (Tarboton, 1997) was used to calculate flow direction, slope (tan $\beta$) and specific catchment area, $a$, for each grid cell in the DEM. This method provides a better estimate of contributing area on hillsides (Tarboton, 1997). The distribution of wetness index, $\ln(a/\tan \beta)$, within each sub-basin was represented using a histogram that recorded the fraction of the sub-basin within each wetness index class. Fig. 4 shows the wetness index and wetness index histograms for a portion of the Blue River watershed.

### 3.2. Temporal inputs

Climate inputs included precipitation at each NEXRAD Stage III radar grid location Radar data was modeled as point rainfall measurements at the center of each $4 \times 4$ km² radar grid cell. Hourly data for air temperature and dew point temperature at each basin gage location, provided by NCDC Cooperate Observer Stations, were adjusted from the gage elevation to the basin average elevation of each sub-basin using lapse rates.
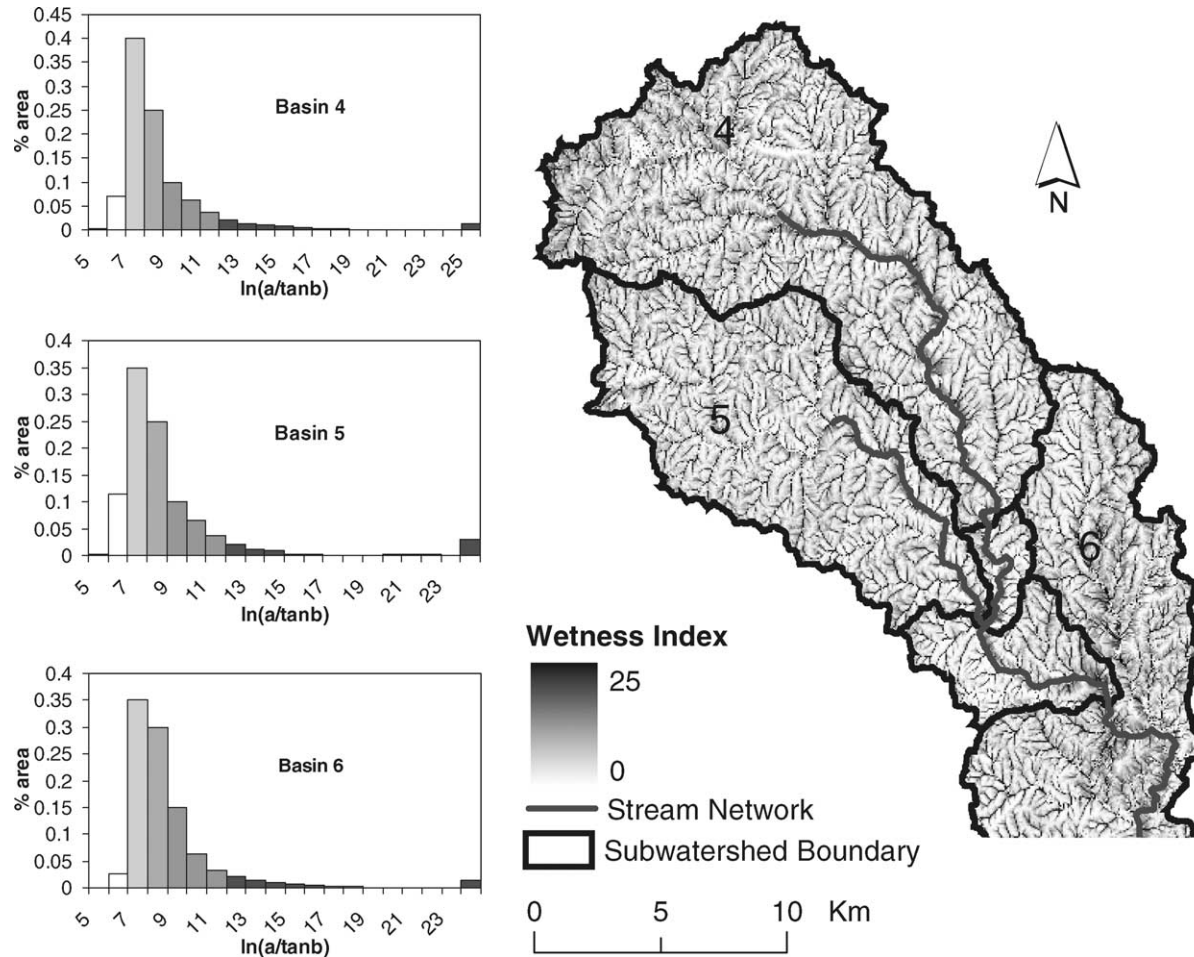
Fig. 4. TOPMODEL wetness index for the upper portion of the Blue watershed. A histogram represents the distribution of wetness index within each sub-basin.

### 3.3. Parameter estimation and calibration

Parameters are time invariant and describe the unchanging properties of the sub-basins or model elements. The parameters of TOPNET are related to physical properties of the sub-basin, including soils, topography, land cover and channel geometry. These are calculated from spatial GIS data and may be spatially uniform, spatially variable and calibrated, or uncalibrated. Table 1 lists the TOPNET model parameters. The third column of Table 1 summarizes how each parameter was estimated in the DMIP experiment. Parameters $f$, $K_0$, $V$, Cr, and $n$, were calibrated for the August 2002 DMIP submission.

Sub-basin model elements have their own distinct model parameters and state variables derived from the soil and vegetation data. The pattern of the spatial variability between sub-basins is maintained during calibration by using multipliers for each parameter that are the same across all sub-basins to scale the Geographic Information System (GIS) derived sub-basin parameters for each sub-basin by the same factor. The calibration procedure uses multipliers, rather than individual sub-basin parameters as its calibration variables. One multiplier value for each parameter applied uniformly to the entire watershed limits the degrees of freedom, and is a parsimonious way to maintain spatial variation

Table 1
TOPNET model parameters

| Sub-basin | Name | Estimation |
|---|---|---|
| $f$ (m$^{-1}$) | Saturated store sensitivity | From soils (multiplier calibrated) |
| $K_0$ (m/h) | Surface saturated hydraulic conductivity | From soils (multiplier calibrated) |
| $\Delta\theta_1$ | Drainable porosity | From soils |
| $\Delta\theta_2$ | Plant available porosity | From soils |
| $d$ (m) | Depth of soil zone | Depth = 1/$f$ from soils |
| $C$ | Soil zone drainage sensitivity | 1 |
| $\psi_f$ (m) | Wetting front suction | From soils |
| $V$ (m/h) | Overland flow velocity | 360 (multiplier calibrated) |
| CC (m) | Canopy capacity | From vegetation |
| Cr | Intercepted evaporation enhancement | From vegetation (multiplier calibrated) |
| $\alpha$ | Albedo | From vegetation |
| Lapse (°C/m) | Lapse rate | 0.0065 |
| *Channel parameters* | | |
| $n$ | Mannings $n$ | 0.024 (multiplier calibrated) |
| $a$ | Hydraulic geometry constant | 0.00011 |
| $b$ | Hydraulic geometry exponent | 0.518 |
| *State variables* | | Initialization |
| $\bar{z}$ (m) | Average depth to water table | Saturated zone drainage matches initial observed flow |
| SR (m) | Soil zone storage | 0.02 |
| CV (m) | Canopy storage | 0.0005 |

between sub-basins based on GIS-derived parameter values.

To prepare TOPNET model input, soils and land cover data were interpolated to the 30 m DEM grid scale. The mapping from soil texture classes and land cover types to model parameters is through a set of value attribute lookup tables, which associate a model parameter value with each 30 m grid cell. Spatial averages of the 30 m grid cell parameter values over the sub-basins that represent model elements are used to obtain the sub-basin parameter values.

Parameters obtained from soil data were derived using soil texture for each of the 11 standard soil depth grid layers from the Pennsylvania (Penn) State University gridding of the NRCS STATSGO database. Fig. 5 shows the derivation of distributed soil based parameters from the soil database. Soil texture from 11 depth based grid layers was associated with each soil class identified using a map unit identifier. The texture of each layer was used to obtain soil parameter values based on the soil hydraulic properties given by Clapp and Hornberger (1978) for each layer. A depth-weighted average was used to calculate the soil class parameter values for drainable porosity, plant available porosity, and wetting front suction. Linear regression of ln($K$) versus depth $z$ was used to fit the assumed exponential function describing decrease of hydraulic conductivity with depth and estimate saturated hydraulic conductivity at the surface, $K_0$ and sensitivity parameter $f$, for each soil class. This regression did not always work because in some soil profiles, hydraulic conductivity increased with depth, or was constant. A lower bound value of $f = 0.667$ m$^{-1}$ was used in these cases corresponding to a soil depth length scale of 1.5 m.

Parameter values for lapse rate, soil zone drainage sensitivity, and hydraulic geometry were left at the default values set in TOPNET, given in Table 1. Parameter values for land cover are given in Table 2. The model was run for an initialization period of 24 days before the DMIP comparison period beginning June 1, 1993, to account for lack of prior knowledge of the initial state variables.

This is the first application that uses this procedure for estimating parameters from STATSGO soil and NASA LDAS vegetation data with TOPNET. There is a scale difference between the sub-basin $K_0$ and $f$ parameters and the point scale parameters inferred from GIS soil texture data. Because of this scale difference, we did not have good default parameters to use in a truly uncalibrated model run and general multiplier values for $f$ and $K_0$ were developed to produce quasi-uncalibrated, or not formally calibrated simulations. Saturated store sensitivity, $f$, is related to streamflow recessions. An average $f$ was obtained by analysis of recessions in the DMIP basins and divided by the average $f$ from the soil data to obtain the default $f$ multiplier for the uncalibrated model runs. Conceptually, the multiplier value relates the average soil $f$ to the average recession $f$. We had hoped to develop an empirical relationship between soil $f$ and recession $f$ using values from each gaged basin, but
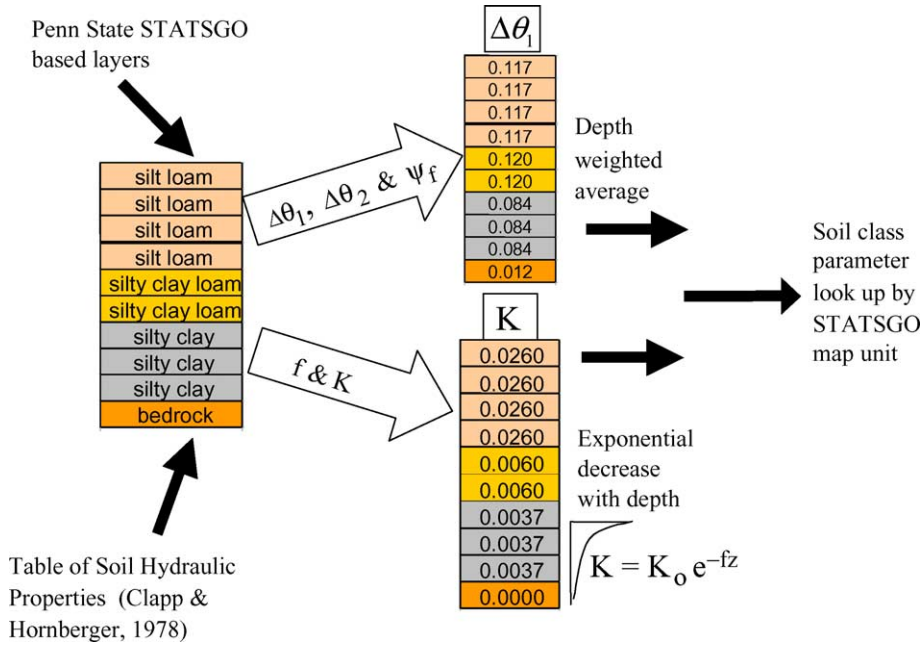
Fig. 5. Derivation of distributed soil based parameters from Penn State soil texture layers derived from STATSGO.

were unsuccessful. The default multiplier value for surface saturated hydraulic conductivity, $K_0$, was selected by trial and error so that, on average, peak flows were of the correct order of magnitude for the DMIP basins. The multiplier values used for uncalibrated model simulations were: (1) saturated store sensitivity, $f$: 6.67, and (2) surface saturated hydraulic conductivity, $K_0$ : 1000. The multipliers for other parameters were held at one for uncalibrated model simulations.

Although the official calibration period for the DMIP experiment was June 1993–May 1999 with a validation period to July 2001, we used a shortened calibration period and calibrated to observed stream flow at the gaged basins for the time period of October 1998–May 1999. We hoped that calibrating to the end of the dataset up to the validation period would avoid incorporating the bias noted in the rainfall prior to 1997 (Seo et al., 1997).

We used the Shuffled Complex Evolution (SCE) algorithm (Duan et al., 1993) implemented in NLFIT (Kuczera, 1983a,b; Kuczera, 1994) to calibrate five selected parameters, (1) saturated store sensitivity, $f$, (2) surface saturated hydraulic conductivity, $K_0$ (3) canopy capacity, CC, (4)

Manning's $n$, and (5) overland flow velocity, $V$. NLFIT is a software package that allows the user to choose parameters for optimization and runs the model for a range of parameter values chosen by

Table 2
Vegetation parameter values derived from land cover data from NASA LDAS vegetation database with IGBP classification of 1-km AVHRR imagery

| Veg class | CC (m) | CR | Albedo | Description |
|---|---|---|---|---|
| 0 | 0 | 1 | 0.23 | Unclassified |
| 1 | 0.003 | 3 | 0.14 | Evergreen needleleaf forest |
| 2 | 0.003 | 3 | 0.14 | Evergreen broadleaf forest |
| 3 | 0.003 | 3 | 0.14 | Deciduous needleleaf forest |
| 4 | 0.003 | 3 | 0.14 | Deciduous broadleaf forest |
| 5 | 0.003 | 3 | 0.14 | Mixed forest |
| 6 | 0.002 | 2 | 0.2 | Closed shrublands |
| 7 | 0.0015 | 1.5 | 0.2 | Open shrublands |
| 8 | 0.0015 | 1.5 | 0.2 | Woody savannah |
| 9 | 0.0015 | 1.5 | 0.2 | Savannahs |
| 10 | 0.001 | 1 | 0.26 | Grasslands |
| 11 | 0.001 | 1 | 0.1 | Permanent wetlands |
| 12 | 0.001 | 1 | 0.26 | Croplands |
| 13 | 0.001 | 1 | 0.3 | Urban/developed |
| 14 | 0.0015 | 1.5 | 0.2 | Natural vegetation |

the SCE algorithm using a global probabilistic search. We used this method to search for multiplier values for each of the calibrated parameters. The unique GIS-derived parameters for each sub-basin were uniformly scaled up or down using the multiplier value derived for the entire watershed. The objective function used in calibration was the mean square error between modeled and observed hourly streamflow. Lack of time and resources limited experiments with different objective functions. The remaining 10 parameters were left uncalibrated due to the model being less sensitive to these parameters and to keep the calibration parsimonious recognizing concerns regarding over-parameterization of distributed models.

## 4. Results and analysis

The model was calibrated using streamflow, once for each of the five DMIP experiment gaged flow locations. The calibration for each DMIP basin used only the downstream gaged location and reserved the interior gaged locations for validation. The number of function evaluations for the search algorithm to minimize the mean square error was as low as 916 for the Elk Basin and as high as 2668 for the Blue Basin.

Results are separated by calibration and validation periods in order to compare the model performance of the two periods, as well as to compare the model performance of calibrated and uncalibrated simulations. The values for calibrated parameter multipliers are given in Table 3 for the five parameters that we calibrated for each DMIP basin, with the corresponding number of function evaluations and

the mean square error for our shortened calibration period. We were able to obtain convergence in all cases, an indication of the robustness of the SCE algorithm. This limited study leaves open future exploration of alternative calibration objectives, improvements in parameter estimation schemes, exploration of non-uniqueness of parameter values and uncertainty in model predictions due to multiple behavioral parameter sets.

### 4.1. Flow prediction

Statistical analyses of the simulations at the calibration streamflow gages are presented in Table 4 for the calibration period and in Table 5 for the validation period. Tables 6 and 7 give statistics at the internal locations not used in calibration. Statistical measures included: modeled average flow, hourly root mean square, mean absolute error, absolute maximum error, Nash–Sutcliffe efficiency measure (NSC), percent bias, and peak difference. Equations for statistical measures are available in (Gupta et al., 1998). Measured average flows are included to provide a reference scale for the results.

Fig. 6 gives a hydrograph comparison for the Illinois River at Tahlequah in 1997. Rainfall is shown as basin average daily totals from NEXRAD data, and hydrograph plots include observed streamflow, simulated streamflow with calibration and simulated streamflow without calibration. This figure is typical of many of the hydrograph comparisons obtained and illustrates some of the challenges faced in this modeling experiment. In some cases, the uncalibrated flows matched peaks better than the calibrated flows; see dates 2/20, 6/1, 7/100 and 8/12 in Fig. 6. Looking at intermediate model outputs (not shown here) reveals

Table 3

Calibrated parameter multipliers and number of function evaluations to converge to the corresponding mean square error using the period October, 1998–May, 1999

|  | *f* | *K* | *V* | Cr | *n* | No. of function evaluations | Mean sq. error (mm/h)$^2$ |
|---|---|---|---|---|---|---|---|
| Baron | 2.9 | 411.9 | 3.2 | 0.8 | 5.0 | 1657 | 0.0023 |
| Blue | 1.7 | 79.9 | 2.4 | 1.1 | 2.4 | 2668 | 0.0017 |
| Elk | 1.6 | 187.6 | 1.8 | 0.8 | 3.6 | 916 | 0.0020 |
| Tahl | 1.8 | 102.7 | 1.8 | 1.0 | 2.8 | 1551 | 0.0011 |
| Watt | 1.5 | 134.3 | 3.3 | 0.9 | 4.4 | 2536 | 0.0015 |

Table 4

Calibrated and uncalibrated results during the June 1, 1993–May 31, 1999 calibration period at streamflow gages used for calibration

| ($m^3$/s) | Calibration period: June 1, 1993–May 31, 1999 | | | | | | | | | |
| | Illinois at Tahlequah | | Illinois at Watts | | Baron Fork at Eldon | | Blue River | | Elk River | |
| | Calibrated | Unclb | Calibrated | Unclb | Calibrated | Unclb | Calibrated | Unclb | Calibrated | Unclb |
|---|---|---|---|---|---|---|---|---|---|---|
| Measured ave flow | 30.38 | 30.38 | 20.92 | 20.92 | 11.78 | 11.78 | 9.83 | 9.83 | 28.89 | 28.89 |
| Modeled ave flow | 35.49 | 32.74 | 24.60 | 22.34 | 13.19 | 12.23 | 15.21 | 13.74 | 38.80 | 35.33 |
| Hourly RMS | 25.11 | 32.91 | 20.11 | 29.72 | 14.73 | 18.82 | 17.24 | 21.93 | 38.65 | 56.74 |
| Mean abs. error | 12.99 | 15.03 | 10.15 | 12.09 | 5.29 | 5.82 | 9.31 | 8.90 | 20.35 | 19.76 |
| Abs. max error | 358.65 | 399.12 | 331.90 | 404.38 | 811.03 | 712.24 | 310.71 | 357.47 | 1398.59 | 1075.51 |
| NSC | 0.71 | 0.51 | 0.68 | 0.31 | 0.71 | 0.53 | 0.53 | 0.25 | 0.53 | −0.02 |
| %Bias | −48.59 | 7.72 | −56.44 | 8.33 | −68.58 | −2.28 | −238.50 | −118.24 | −135.08 | −27.83 |
| Peak difference | 168.12 | 3.38 | 191.57 | 108.04 | 103.12 | 164.14 | −98.27 | −117.54 | 1381.22 | 285.72 |

Table 5

Calibrated and uncalibrated results during the June 1, 1999–July 31, 2000 validation period at streamflow gages used for calibration

| ($m^3$/s) | Validation period: June 1, 1999–July 31, 2000 | | | | | | | | | |
| | Illinois at Tahlequah | | Illinois at Watts | | Baron Fork at Eldon | | Blue River | | Elk River | |
| | Calibrated | Unclb | Calibrated | Unclb | Calibrated | Unclb | Calibrated | Unclb | Calibrated | Unclb |
|---|---|---|---|---|---|---|---|---|---|---|
| Measured ave flow | 30.91 | 30.91 | 19.63 | 19.63 | 9.59 | 9.59 | 2.25 | 2.25 | 19.05 | 19.05 |
| Modeled ave flow | 38.25 | 34.30 | 24.69 | 21.57 | 10.53 | 9.34 | 9.04 | 6.60 | 36.89 | 31.69 |
| Hourly RMS | 34.73 | 34.11 | 26.79 | 32.75 | 17.94 | 26.22 | 9.83 | 11.32 | 28.46 | 44.62 |
| Mean abs. error | 15.63 | 12.79 | 10.81 | 10.59 | 4.33 | 4.72 | 6.83 | 4.73 | 20.15 | 15.65 |
| Abs. max error | 416.95 | 666.95 | 459.10 | 421.72 | 828.58 | 944.58 | 171.59 | 169.35 | 391.99 | 488.90 |
| NSC | 0.81 | 0.81 | 0.78 | 0.67 | 0.84 | 0.67 | −13.64 | −18.44 | 0.59 | −0.02 |
| %Bias | −57.56 | 10.52 | −55.39 | 15.94 | −56.26 | 14.59 | −381.56 | −172.77 | −199.08 | −31.57 |
| Peak difference | 181.69 | −299.57 | 195.47 | 13.66 | 547.44 | 823.33 | −135.42 | −133.16 | 251.36 | −226.43 |

Table 6

Calibrated and uncalibrated results during the June 1, 1993–May 31, 1999 calibration period at interior locations modeled as 'ungaged'

| ($m^3$/s) | Calibrated at Tahlequah | | | | Calibrated at Eldon | |
| | Illinois at Watts | | Flint Creek | | Peacheater Creek | |
| | Calibrated | Unclb | Calibrated | Unclb | Calibrated | Unclb |
|---|---|---|---|---|---|---|
| Measured ave flow | 20.92 | 20.92 | 3.28 | 3.28 | 0.70 | 0.70 |
| Modeled ave flow | 23.97 | 22.10 | 3.88 | 3.57 | 1.03 | 0.96 |
| Hourly RMS | 20.90 | 30.26 | 4.25 | 5.61 | 1.25 | 1.93 |
| Mean abs. error | 9.55 | 12.34 | 1.71 | 2.04 | 0.50 | 0.53 |
| Abs. max error | 395.39 | 415.29 | 231.66 | 249.85 | 37.68 | 57.21 |
| NSC | 0.66 | 0.28 | 0.51 | 0.15 | 0.26 | −0.75 |
| %Bias | −41.69 | 8.76 | −44.73 | 8.02 | −49.58 | −39.31 |
| Peak difference | 240.23 | 165.38 | 203.54 | 173.77 | 5.70 | −10.42 |

Table 7
Calibrated and uncalibrated results during the June 1, 1999–July 31, 2000 validation period at interior locations modeled as 'ungaged'

| (m³/s) | Calibrated at Tahlequah | | | | | |
| | Illinois at Watts | | Flint Creek | | Peacheater Creek | |
| | Calibrated | Unclb | Calibrated | Unclb | Calibrated | Unclb |
|---|---|---|---|---|---|---|
| Measured ave flow | 19.63 | 19.63 | 3.86 | 3.86 | 0.61 | 0.61 |
| Modeled ave flow | 24.38 | 21.78 | 4.55 | 4.14 | 0.91 | 0.81 |
| Hourly RMS | 28.33 | 35.01 | 12.76 | 14.60 | 1.54 | 2.41 |
| Mean abs. error | 10.46 | 11.13 | 2.40 | 2.92 | 0.42 | 0.45 |
| Abs. max error | 457.69 | 413.40 | 459.65 | 478.14 | 63.51 | 71.97 |
| NSC | 0.75 | 0.62 | 0.45 | 0.28 | 0.80 | 0.50 |
| %Bias | −40.53 | 13.87 | −46.42 | 7.97 | −48.70 | −31.54 |
| Peak difference | 257.61 | 96.85 | 429.57 | 410.78 | 59.76 | 63.95 |

that the baseflow from the uncalibrated model tends to better match the observed streamflow. The difference between model and observed baseflow after calibration is a significant contributor to the bias reported in Tables 4–7. There are also peaks in the simulated streamflow due to what appear to be significant basin average daily rainfall totals in excess of 20 mm, where little or no observed streamflow peak occurs. These may be due to the radar overestimating the rainfall input, or to snow, which had not been incorporated into

TOPNET at the time of these model simulations, or due to limitations in the models ability to represent antecedent conditions and discern whether or not the basin is primed to respond to rainfall.

The values for the Nash–Sutcliffe efficiency reported in Tables 4 and 5 (parent basins) and Tables 6 and 7 (interior locations) are different from the values in Table 9 of Reed et al. (2003) since our statistical measures are reported for the calibration and validation periods separately. Using
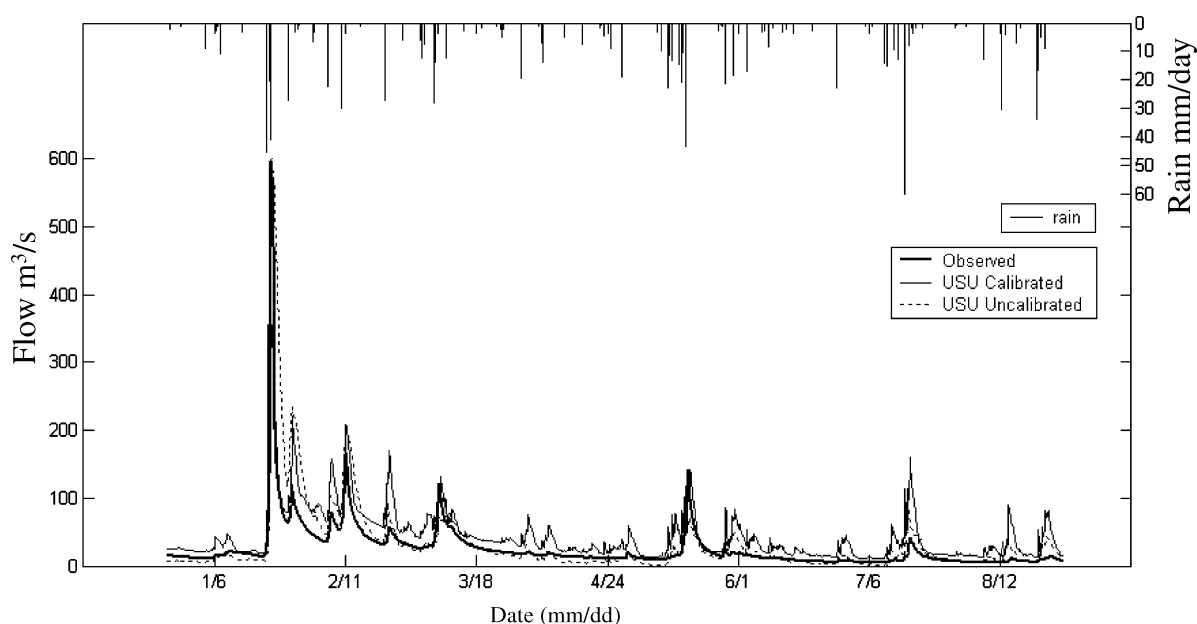


Fig. 6. Hydrograph for the Illinois River at Tahlequah for flows from January, 1997 to August, 1997.

the Nash–Sutcliffe efficiency, where a value of 1 represents a perfect fit and values less than 0.7 are generally considered unacceptable, one can see that many of our simulations would be deemed unacceptable. One can also see that both our calibrated and uncalibrated model simulations are better in the validation period than over the calibration period, with the exception of the Blue River. The improved model performance in the validation period is possibly due to the fact that we calibrated our models only to the portion of the streamflow record immediately before the validation period that is more similar to the validation period than the entire calibration period. There is also variability in model performance measures due to the differences in precipitation and streamflow patterns between calibration and validation periods.

In Tables 4 and 5, there is a notable difference in the relatively better performance at Illinois at Tahlequah, Illinois at Watts, and the Baron Fork at Eldon compared to the poor performance at the Elk River watershed and Blue River, Oklahoma. Looking at the Nash–Sutcliffe efficiency and bias results, one can see that the Nash–Sutcliffe efficiency is improved by calibration. This is expected with the use of mean-square error as an objective during calibration. This improvement in mean square error comes at a cost, however, in terms of increased bias associated with the calibrated flows. The statistical improvement does not therefore necessarily reflect an improvement in terms of simulated hydrographs. This was evident in Fig. 6 where, although the calibration resulted in better fitting of some high peak flows which dominate the mean square error differences, calibration resulted

in an overall increase in modeled flows and decreased the quality of model performance during average and low flow periods.

The percent bias, calculated for the entire experimental period (calibration and validation periods), is presented in Figs. 7 and 8, where the calibration (Fig. 7) created a model that fits the high spring flows, but that causes over-prediction during the rest of the year, during lower flow periods. The uncalibrated results (Fig. 8) show the tendency of the model to over-predict streamflow in the first three months of the water year, and then to under-predict during the higher flow periods.

### 4.2. Using distributed models to simulate flow at uncalibrated interior locations

There are three DMIP interior locations that were modeled as 'ungaged' but have measured streamflow to use for testing model results. The comparison of model performance in the additional five ungaged locations are presented using the coefficient of variation to compare with the models in Reed et al. (2003). Tables 6 and 7 present the statistical results for the interior locations with measured streamflow not available for calibration. Using the Nash–Sutcliffe coefficient as a measure, the calibrated model did well modeling the high flows at Peacheater Creek, especially during the validation period. This result is encouraging since the June flood event was greater than 100 times the average low flows in the creek (Fig. 9a). However, the effect of calibration on the peak flows can be seen when a log scale is used, Fig. 9b and c. Fig. 9c
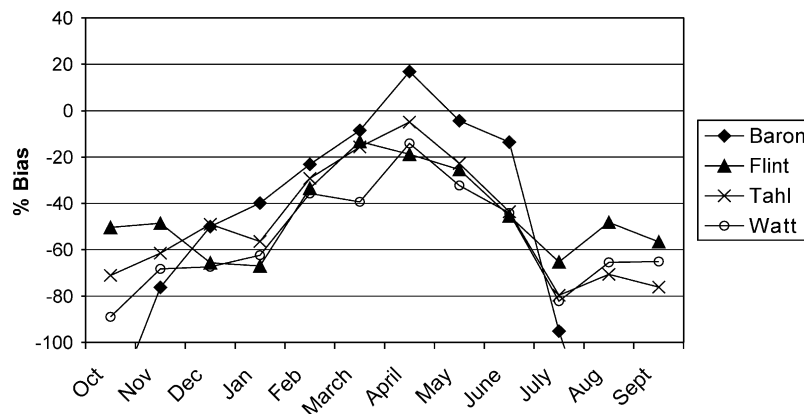


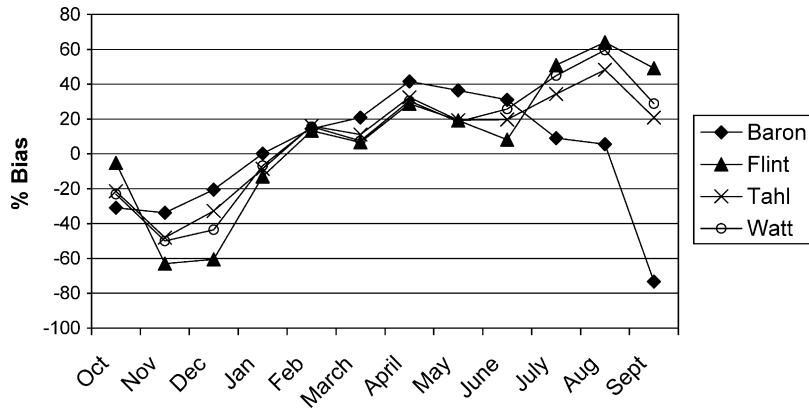Fig. 7. Percent bias of calibrated results by month for selected DMIP watersheds.

Fig. 8. Percent bias of uncalibrated results by month for selected DMIP watersheds.

shows the streamflow for this period in the Baron Fork at Eldon. This is the streamflow location used in calibration. High flows dominate the mean square error objective and Nash–Sutcliffe efficiency measure. The high flows in Fig. 9c are well matched, suggesting that the physical processes involved in the generation of high flows have been sufficiently captured by the model to carry over into an out of sample validation period. This matching of high flows also carries over to the interior Peacheater Creek location.
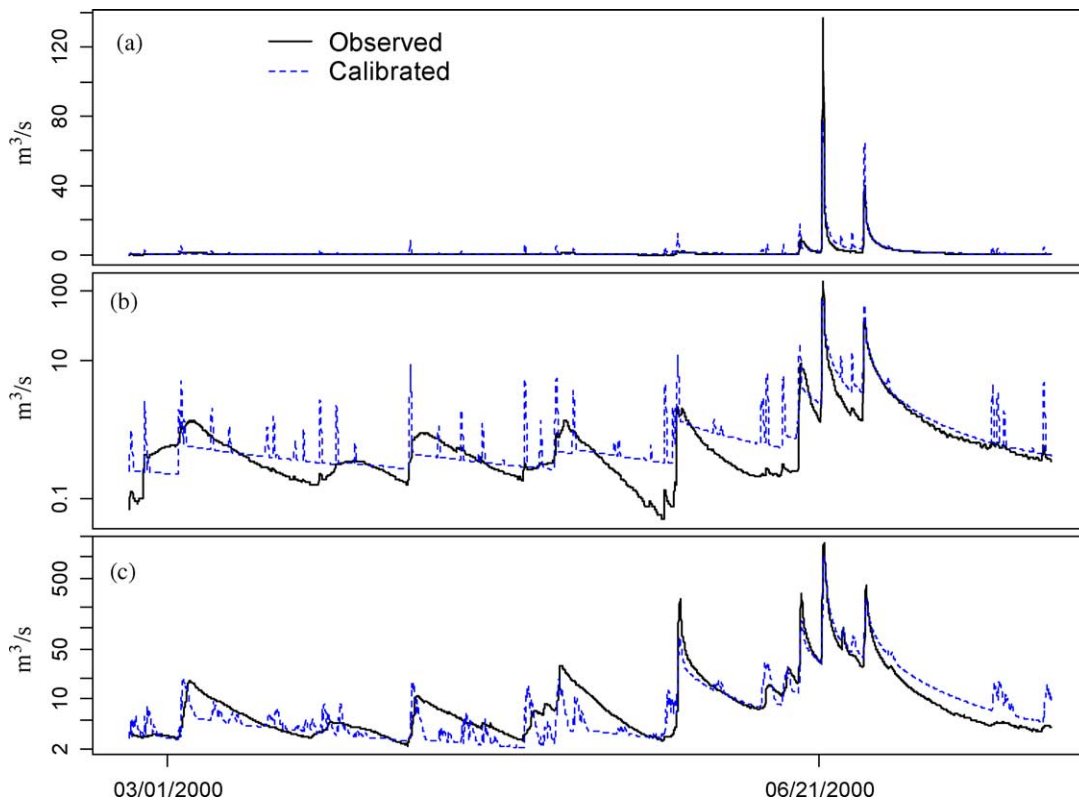


Fig. 9. (a) Peacheater Creek calibrated streamflow results, (b) Peacheater Creek calibrated log streamflow results, and (c) Baron Fork at Eldon log streamflow results for the 1999–2000 validation period.

The low flow recessions are not modeled well, either at Baron Fork (Fig. 9c) or Peacheater Creek (Fig. 9b). TOPMODEL has a single function that models baseflow recession, Eq. (10). The calibration has resulted in the adjustment of the sensitivity parameter $f$ to match high flow recessions rather than low flow recessions. Jakeman and Hornberger (1993) identified the need for rainfall runoff models to include both a quick flow and slow flow response. In TOPMODEL, as it is functioning in the sub-surface storage component of TOPNET, the response is being controlled by the single exponential discharge–storage function that is unable to represent both high and low flow recessions. Furthermore, the recessions in Fig. 9b and c on the log scale appear close to linear suggesting that linear discharge–storage, rather than exponential discharge–storage functions may be better for this watershed. These results indicate that if the full range of streamflow is to be simulated successfully a more flexible parameterization of the discharge–storage function is required, perhaps along the lines of Lamb and Beven (1997) or Duan and Miller (1997). Using validation periods and interior locations for testing model performance of distributed models has helped us test our model assumptions and their impact on simulation of streamflow. The DMIP intercomparison experiment has proven to be a valuable and important framework for assessment of model performance before

operational or other model applications are implemented.

### 4.3. Using radar rainfall for distributed modeling

The propagation of radar-rainfall estimation errors through runoff predictions should be estimated. Unfortunately, because all available rain gage data was used in the generation of NEXRAD Stage III data, there is no independent data to assess the accuracy of this data (Seo et al., 1997; Young et al., 2000). Examples of limitations are well documented in the literature (Smith et al., 1996; Young et al., 2000). Lack of information on the uncertainty in radar rainfall inputs does limit the interpretation of model performance based on statistical measures, especially over time-scales longer than the single event.

### 4.4. Diagnosis of TOPNET using DMIP results

One of the benefits of distributed hydrologic modeling is the spatial variation of intermediate calculations and model results. Participation in the DMIP experiment has provided a good way to test the strengths and weaknesses of TOPNET and point towards directions for model improvements. In Figs. 10–14, we use November–December data from 1994 for the Baron Fork at Eldon as an example of how we perform model diagnosis using
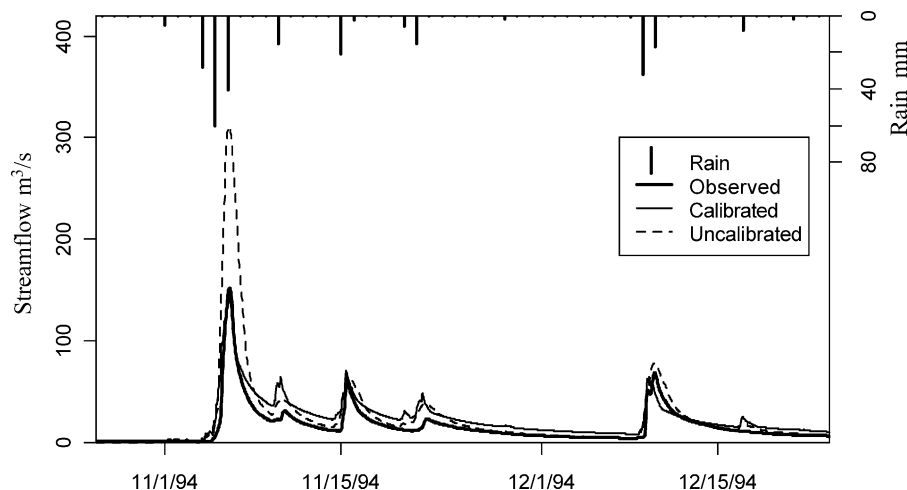


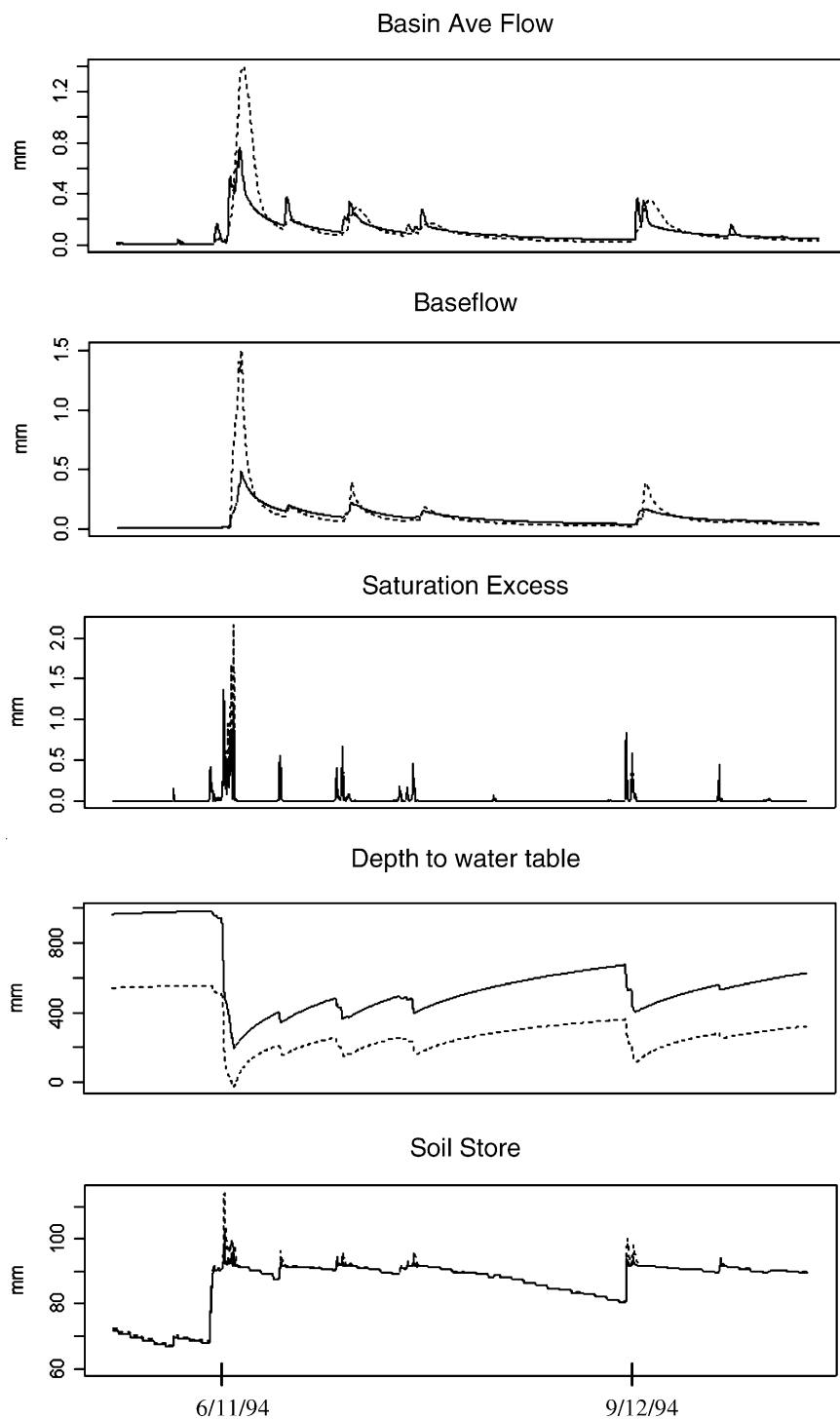Fig. 10. Calibrated and uncalibrated simulated streamflow for Baron Fork at Eldon, November 1994.

Fig. 11. Calibrated (——) and uncalibrated (- - -) watershed averaged model components for Baron Fork at Eldon, at the beginning of the water year 10/25/1994–12/20/1994.
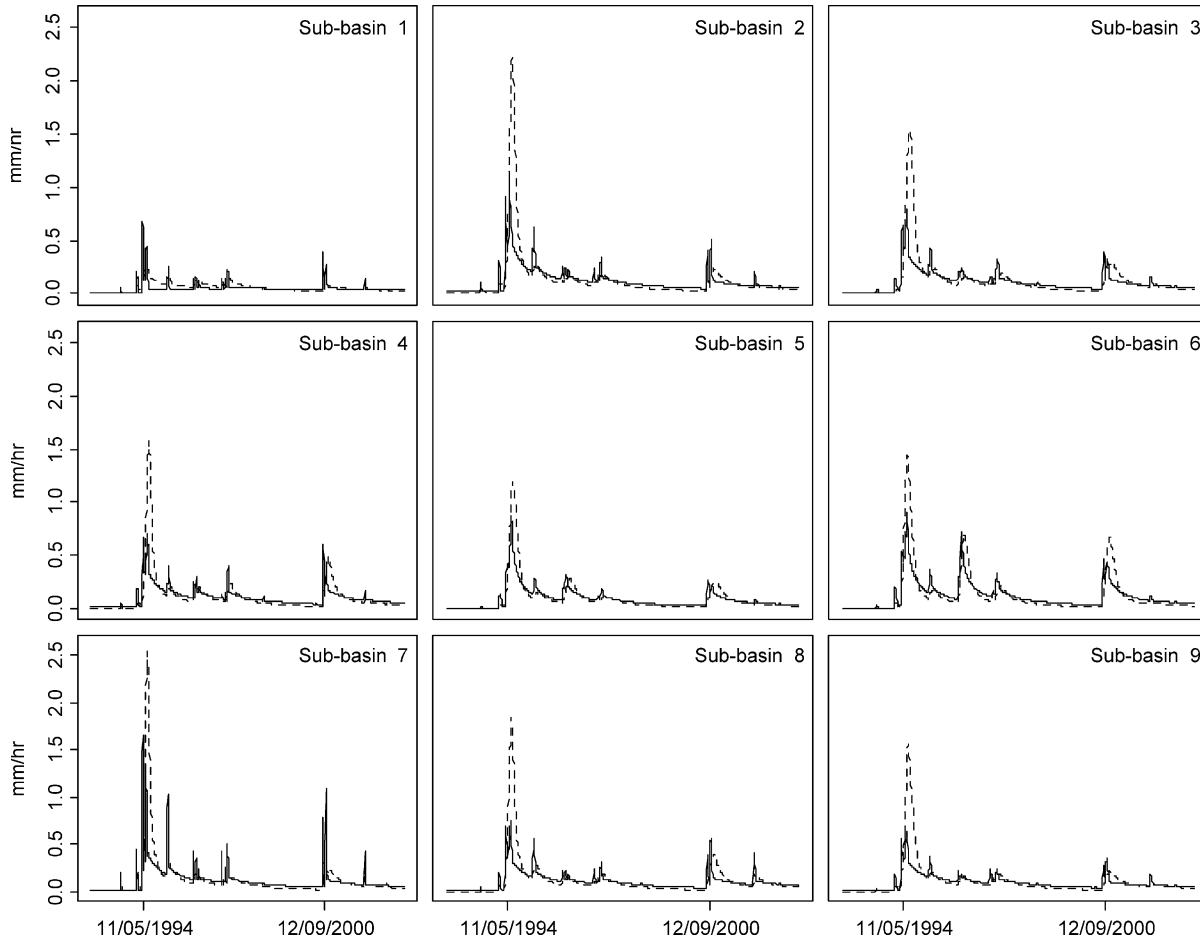
Fig. 12. Calibrated (—) and uncalibrated (- - -) direct streamflow by sub-watershed for Baron Fork at Eldon, at the beginning of the water year 10/25/1994–12/20/1994.

the different modeled responses captured by calibrated and uncalibrated results. This time period is presented since the temporal shift in bias with over-prediction in the early part of the water year was of special interest. We wanted to check whether this bias is a function of radar input bias, model structure, or soil parameterization.

In Fig. 10, the hydrograph for the time period shows that the calibrated result fits the peak event in the beginning of November, and the uncalibrated result over-estimates the peak flow. Fig. 10 also shows that the calibrated result over-predicts the low flows while the uncalibrated flow fits the low flows and recessions better. An investigation of how the model is partitioning the flows can be conducted by checking

the basin averaged model component results during the time period. Fig. 11 shows the averages of sub-basin outputs for some TOPNET diagnostic variables, this is an aggregate view of model response. The calibrated and uncalibrated models have different basin averaged flow, baseflow, saturation excess runoff, depth to the water table, $\bar{z}$, and soil zone storage. Canopy storage, evapotranspiration, and infiltration excess were also investigated but these results are not shown because the calibrated and uncalibrated modeling of these components was not significantly different.

Fig. 12 shows the streamflow originating from each individual sub-basin, indicating that the difference in modeled response can be traced to specific sub-basins.
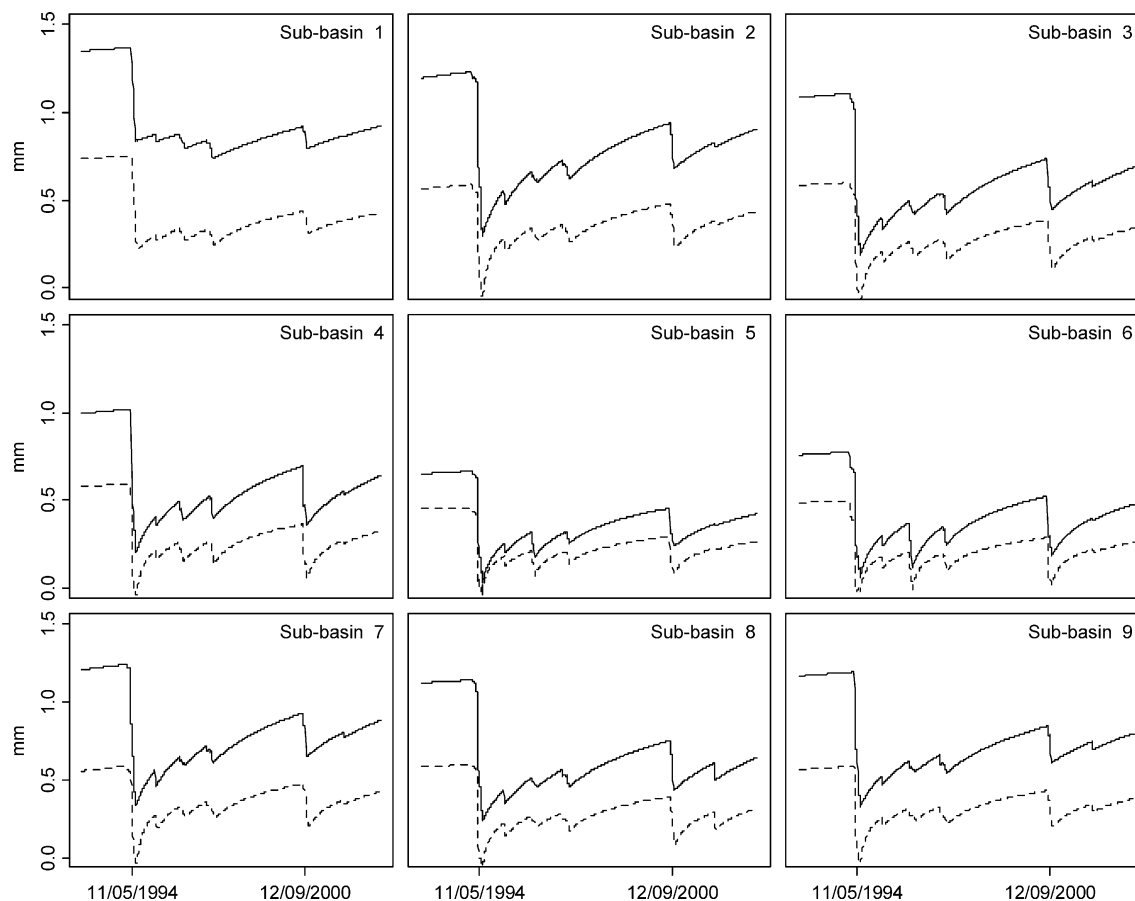
Fig. 13. Calibrated (—) and uncalibrated (- - -) depth to the water table by sub-watershed for Baron Fork at Eldon, at the beginning of the water year 10/25/1994–12/20/1994.

Sub-basin one does not contribute to the difference in flow between calibrated and uncalibrated simulations while all the other sub-basins do, to a varying degree. The parameters to which basin response is most sensitive are $K_0$ and $f$. These are reported in Table 8 for each sub-basin within the Baron Fork at Eldon watershed. This table also presents the calibration and default (uncalibrated) multipliers that were used to obtain these parameters from those derived directly from the soils data. Most notable is that overall the $f$ parameter is larger for the uncalibrated than for the calibrated simulations.

The streamflow response in these model simulations is dominated by baseflow and saturation excess runoff. Baseflow responds at short time scales representing the sub-surface streamflow response.

Saturation excess is due to precipitation on saturated areas where the wetness index is large. The simulated extent of saturated area is related to the simulated depth to the water table and increases as the depth to the water table decreases. Fig. 13 shows the depth to the water table modeled in each basin. A large $f$, acting through Eq. (10), makes the baseflow from a sub-basin more sensitive to changes in depth to water table and hence more sensitive to precipitation inputs. This is the main reason why, in general, the uncalibrated simulations are flashier. However, because of the non-linear exponential form of Eq. (10), sensitivity to $\bar{z}$ depends upon changes in $\bar{z}$ in a multiplicative, rather than additive way. A change in $\bar{z}$ by $\Delta\bar{z}$ results in multiplication of baseflow by a factor $e^{-f\Delta\bar{z}}$. If baseflow is small, the change is still
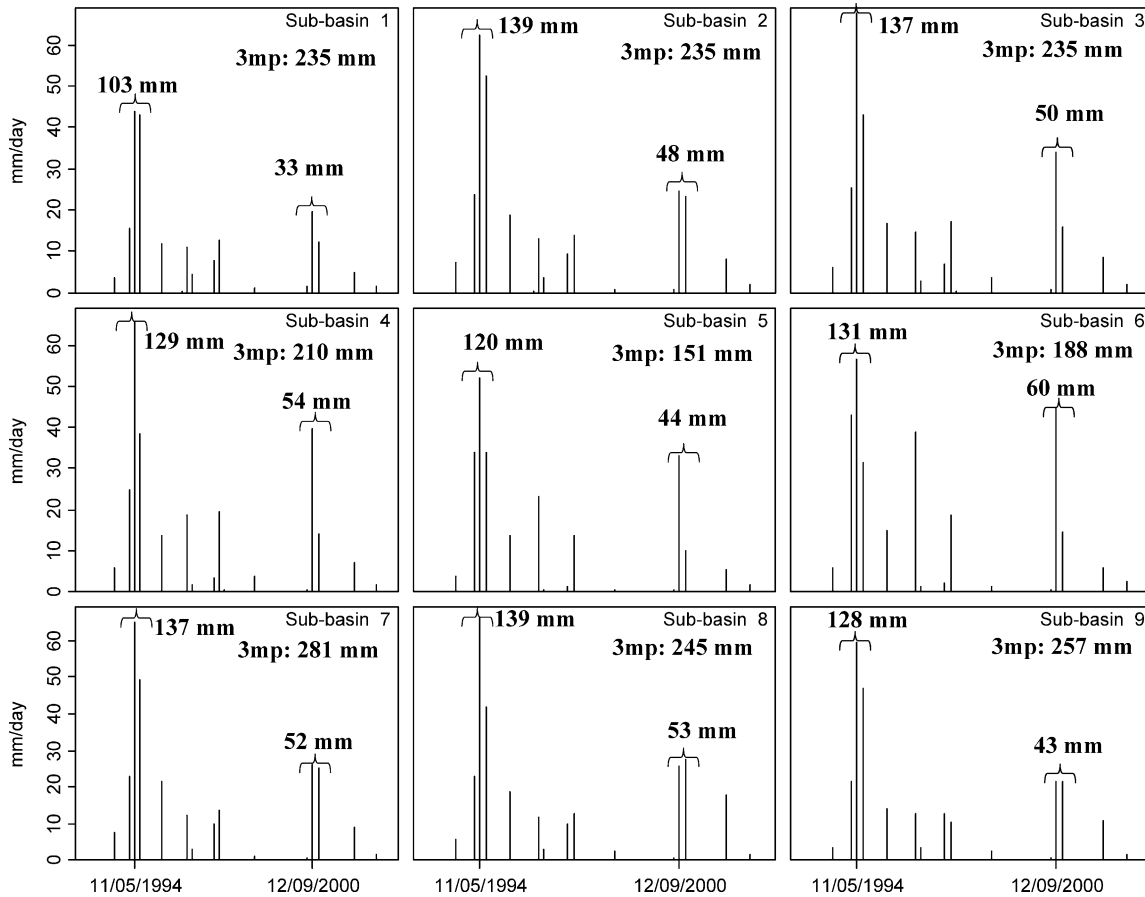
Fig. 14. Radar rain sub-watershed averages for Baron Fork at Eldon, at the beginning of the water year 10/25/1994–12/20/1994.

small in absolute terms. If, however, baseflow is large, the change is large.

The specific degree to which a sub-basin is more or less flashy in uncalibrated versus calibrated simulations depends upon the juxtaposition of precipitation, antecedent precipitation and basin parameters. Fig. 14 shows the sub-basin rainfall in each sub-basin with the three-day storm totals associated with the 11/6/94 and 12/9/94 events, as well as the prior three-month antecedent precipitation. Sub-basin one has the smallest rainfall totals for this two-month period. Initial depth to water table is largest with the result that increases in soil moisture do not significantly increase the saturated area. The baseflow response from sub-basin one in both simulations is relatively minor due to the sensitivity multiplier being applied to a small

Table 8
Baron Fork at Eldon $f$ and $K_0$ sub-basin parameters

|  | Calibrated | | Uncalibrated | |
|---|---|---|---|---|
| Multipliers | 2.9 | 411.9 | 6.7 | 1000 |
| Sub-basin | $f$ (m$^{-1}$) | $K_0$ (m/h) | $f$ (m$^{-1}$) | $K_0$ (m/h) |
| 1 | 3.76 | 12.4 | 8.69 | 30.0 |
| 2 | 3.80 | 12.4 | 8.78 | 30.2 |
| 3 | 4.02 | 12.4 | 9.29 | 30.0 |
| 4 | 4.57 | 12.9 | 10.57 | 31.4 |
| 5 | 7.93 | 22.8 | 18.31 | 55.4 |
| 6 | 6.72 | 20.4 | 15.53 | 49.6 |
| 7 | 3.73 | 12.4 | 8.63 | 30.0 |
| 8 | 4.19 | 12.3 | 9.68 | 29.8 |
| 9 | 4.14 | 12.4 | 9.57 | 30.2 |

number. Sub-basins five and six have different soils that result in them having different $f$ and $K_0$ parameters. The larger values of $f$ should imply large sensitivity, but the large sensitivity results in the saturated zone adjusting rapidly to accommodate inputs. As soon as $\bar{z}$ decreases due to water entering the saturated zone, the baseflow increases modulating the reduction in $\bar{z}$. This effect limits the range over which $\bar{z}$ varies for these sub-basins, as indicated in Fig. 13. The $f$ values for sub-basins five and six are sufficiently large that this behavior is similar for both calibrated and uncalibrated simulations. In the remaining sub-basins, the depth to water table is such that streamflow is quite sensitive to decreases in $\bar{z}$. The sub-basins with the largest precipitation inputs (two, three and seven) that follow the largest antecedent precipitation inputs are most sensitive and exhibit the largest differences between calibrated and uncalibrated results.

We do not know, for these watersheds, how much of this model behavior is representative of reality. We also do not know whether the rainfall inputs are sufficiently resolved at the scale of sub-basins to meaningfully drive differences in sub-basin response. Distributed modeling studies like this stimulate questions and hypotheses that can be pursued further in the ongoing effort to better understand and model the hydrologic response of watersheds. We have confirmed that for TOPNET, with TOPMODEL controlling sub-surface flow, the parameter f is highly sensitive and its derivation from GIS soils information and careful calibration of the multiplier value is important for accurate streamflow simulations.

### 4.5. Model run-time

Computer and time resources remain a limiting factor to the operational use of distributed models. Our computer system for the work was an AMD athlon XP 1900 + with 512 MB RAM, 1.4 GHz, and Windows 2000 platform. Run-time for one seven-year model run of 63,000 hourly timestep was 4–9 min for a range of 9–21 model elements. Time for parameter calibration by the SCE algorithm incorporated in the NLFIT software for five parameters took between 6 and 9 h. See Table 9 for computer run times required to model each of the DMIP basins.

Table 9
Model run time and calibration time for each of the DMIP basins

| Basin | Model elements | Run-time minutes/model run | Parameter calibration (h) |
|---|---|---|---|
| Baron | 9 | 4 | 6 |
| Blue | 9 | 7 | 6 |
| Elk | 16 | 6 | 8 |
| Tahl | 21 | 9 | 9 |
| Watt | 15 | 7 | 7 |

## 5. Discussion and conclusion

For both calibration and validation periods, we found that for our model calibrated flows using the mean square error objective function improved the matching of the peak streamflows, at the cost of over-predicting the low flows and introducing bias into the cumulative water balance, shown in the different results for calibrated and uncalibrated simulations. Statistics based on the square of the error term are highly sensitive to differences between model and measured flow during peak flood flows. Overall, the model performed as well, or better in some cases, in the validation period as in the calibration period. Lack of information on the uncertainty in radar rainfall inputs limited the interpretation of statistical performance measures used in DMIP to verify the quality of flood simulations. Similarly, this lack of information would limit the useful interpretation of statistical performance measures used to verify the quality of flood forecasts in applications beyond the scope of this project.

The use of distributed models to simulate flow at ungaged interior locations was highlighted with the model results in Peacheater Creek at Christie, Oklahoma. Our model simulations with calibration were as good at interior locations, especially during the validation period, as in the larger scale basins. Understanding the reasons for the difference in relative performance in larger basins and in interior locations compared to the distributed Sacramento models will help us improve our model simulations for all basin scales. Comparative studies between the model structures for simulating the sub-surface (TOPMODEL versus Sacramento), treatment of

radar rain sub-basin averaging, and soil parameterization should be conducted.

The exponential functional form of baseflow discharge–storage response limits the capability of our model to match recessions in both low and high flow scenarios and a single value per sub-basin for the $f$ parameter may not be appropriate. If the full range of streamflow is to be simulated successfully a more flexible parameterization of the discharge–storage function is required, perhaps including separate quick flow and slow flow functionality (Jakeman and Hornberger, 1993) or development of a generalized discharge–storage function from actual recession curve analysis (Lamb and Beven, 1997), or by generalizing the discharge–storage function (Duan and Miller, 1997).

The small difference between calibrated and uncalibrated results for TOPNET showed that, in some basins, flows could be predicted well with little or no calibration. Interior gages were modeled comparatively as well as calibrated gages and show the benefit of distributed models for simulating uncalibrated interior monitoring point locations. In future work we intend to investigate model element scale questions and sensitivity to the spatial data resolution of soil and vegetation data. We would like to increase the number of model elements to see if smaller element size improves model performance. Since the submission of DMIP results in August 2000, we have added an impervious area parameter to the model structure and will be testing this functionality in urban and disturbed watersheds.

## Acknowledgements

## References

Beven, K.J., Kirkby, M.J., 1979. A physically based variable contributing area model of basin hydrology. Hydrological Sciences Bulletin 24(1), 43–69.

Beven, K., Lamb, R., Quinn, P., Romanowicz, R., Freer, J., 1995a. Topmodel. In: Singh, V.P., (Ed.), Computer Models of Watershed Hydrology, 18. Water Resources Publications, Highlands Ranch, CO, (Chapter 18); pp. 627–668.

Beven, K., Quinn, P., Romanowicz, R., Freer, J., Fisher, J., Lamb, R., 1995b. Topmodel and Gridatb, a Users Guide to the Distribution Versions (95.02), CRES Technical Report TR110, Centre for Research on Environmental Systems and Statistics, Institute of Environmental and Biological Sciences, Lancaster University, Lancaster.

Bristow, K.L., Campbell, G.S., 1984. On the relationship between incoming solar radiation and the daily maximum and minimum temperature. Agricultural and Forest Meteorology 31, 159–166.

Brooks, R.H., Corey, A.T., 1966. Properties of porous media affecting fluid flow. Journal of Irrigation and Drainage ASCE 92(IR2), 61–88.

Broscoe, A.J., 1959. Quantitative analysis of longitudinal stream profiles of small watersheds. Office of Naval Research, Project NR 389-042. Technical Report No. 18, Department of Geology, Columbia University, New York.

Clapp, R.B., Hornberger, G.M., 1978. Empirical equations for some soil hydraulic properties. Water Resources Research 14, 601–604.

Dingman, S.L., 2002. Physical Hydrology, second ed., Prentice Hall, Englewood Cliffs, NJ, 646 pp.

Duan, J., Miller, N.L., 1997. A generalized power function for the subsurface transmissivity profile in TOPMODEL. Water Resources Research 33, 2559–2562.

Duan, Q., Gupta, V.K., Sorooshian, S., 1993. A shuffled complex evolution approach for effective and efficient global minimization. Journal of Optimization Theory and Its Applications 76(3), 501–521.

Eidenshink, J.C., Faundeen, J.L., 1994. The 1-Km avhrr global land data set: first stages in implementation. International Journal of Remote Sensing 15, 3443–3462.

Famiglietti, J.S., Wood, E.F., 1994a. Application of multiscale water and energy balance models on a Tallgras Prairie. Water Resources Research 30(11), 3079–3093.

Famiglietti, J.S., Wood, E.F., 1994b. Mutiscale modeling of spatially variable water and energy balances. Water Resources Research 30(11), 3061–3078.

Famiglietti, J.S., Wood, E.F., Sivapalan, M., Thongs, D.J., 1992. A catchment scale water balance model for fife. Journal of Geophysical Research 97(D17), 18997–19007.

Flint, J.J., 1974. Stream gradient as a function of order, magnitude and discharge. Water Resources Research 10(5), 969–973.

Goring, D.G., 1994. Kinematic shocks and monoclinal waves in the Waimakariri, a steep, braided, gravel-bed river, Proceedings of the International Symposium on Waves: Physical and Numerical Modelling, University of British Columbia, Vancouver, Canada, 21–24 August, 1994, pp. 336–345.

Gupta, H.V., Sorooshian, S., Yapo, P.O., 1998. Toward improved calibration of hydrologic models: multiple and noncommensurable measures of information. Water Resources Research 24(4), 751–763.

Ibbitt, R., 1971. Development of a conceptual model of interception, Unpublished Hydrological Research Progress Report No. 5, Ministry of Works, New Zealand.

Jakeman, A.J., Hornberger, G.M., 1993. How much complexity is warranted in a rainfall-runoff model. Water Resources Research 29(8), 2637–2649.

Kuczera, G., 1983a. Improved parameter inference in catchment models. 1. Evaluating parameters. Water Resources Research 19(5), 1151–1162.

Kuczera, G., 1983b. Improved parameter inference in catchment models. 2. Combining different kinds of hydrologic data and testing their compatibility. Water Resources Research 19(5), 1162–1172.

Kuczera, G., 1994. Nlfit, a Bayesian Nonlinear Regression Program Suite, Version 1.00g, Department of Civil Engineering and Surveying, University of Newcastle, New South Wales.

Lamb, R., Beven, K., 1997. Using interactive recession curve analysis to specify a general catchment storage model. Hydrology and Earth Systems Science 1, 101–113.

Leopold, L.B., Maddock, T., 1953. The hydraulic geometry of stream channels and some physiographic implications. US Geological Survey Professional Paper, No. 252.

Priestley, C.H.B., Taylor, R.J., 1972. On the assessment of surface heat flux and evaporation using large-scale parameters. Monthly Weather Review 100(2), 81–92.

Reed, S., Koren, V., Smith, M., Zhang, Z., Moreda, F., Seo, D.-J., 2004. Overall distributed model intercomparison project results, Journal of Hydrology 298(1–4), 27–60.

Rutter, A.J., Kershaw, K.A., Robins, P.C., Morton, A.J., 1972. A predictive model of rainfall interception in forests. 1. Derivation of the model from observations in a plantation of Corsican Pine. Agricultural Meteorology 9, 367–384.

Seo, D.J., Fulton, R.A., Breidenbach, J.P., 1997. Final Report for Interagency MOU among the Nexrad Program, WSR-88D OSF and NWS/OH/HRL, NWS/OH/HRL, Silver Spring, MD.

Shuttleworth, W.J., 1993. Evaporation. In: Maidment, D.R., (Ed.), Handbook of Hydrology, McGraw-Hill, New York, (Chapter 4).

Smith, M., 2002. Distributed model intercomparison project (Dmip). National Weather Service. Retrieved October, 2001 from the World Wide Web: http://www.nws.noaa.gov/oh/hrl/dmip/.

Smith, J.A., Seo, D.J., Baeck, M.L., Hudlow, M.D., 1996. An intercomparison study of nexrad precipitation estimates. Water Resources Research 32, 2035–2045.

Soil Survey Staff, 1994a. State Soil Geographic Database (Statsgo) Collection for the Conterminous United States, USDA-NRCS, National Soil Survey Center, Lincoln, NE, CD-ROM.

Soil Survey Staff, 1994b. State Soil Geographic Database (Statsgo) Data Users Guide Miscellaneous Publication 1492, USDA Natural Resources Conservation Service, US Government Printing Office, Washington, DC, p. 88.

Stewart, J.B., 1977. Evaporation from the wet canopy of a pine forest. Water Resources Research 13(6), 915–921.

Tarboton, D.G., 1997. A new method for the determination of flow directions and contributing areas in grid digital elevation models. Water Resources Research 33(2), 309–319.

Tarboton, D.G., 2002. Terrain Analysis Using Digital Elevation Models (Taudem), Utah Water Research Laboratory, Utah State University, http://www.engineering.usu.edu/dtarb.

Tarboton, D.G., Ames, D.P., 2001. Advances in the mapping of flow networks from digital elevation data, World Water and Environmental Resources Congress, Orlando, FL, May 20–24, 2001, ASCE.

USGS, 2003. The National Map Seamless Data Distribution Server, EROS Data Center, http://seamless.usgs.gov/.

Young, C.B., Bradley, A.A., Krajewski, W.F., Kruger, A., 2000. Evaluating nexrad multisensor precipitation estimates for operational hydrologic forecasting. Journal of Hydrometeorology 1, 241–254.